Aquaporin-4 facilitator TGN-073 promotes interstitial fluid circulation within the blood–brain barrier: [^{17}O]H_2O JJVCPE MRI study

Vincent J. Huber[a,*], Hironaka Igarashi[a,*], Satoshi Ueki[a], Ingrid L. Kwee[a,b] and Tsutomu Nakada[a,b]

The blood–brain barrier (BBB), which imposes significant water permeability restriction, effectively isolates the brain from the systemic circulation. Seemingly paradoxical, the abundance of aquaporin-4 (AQP-4) on the inside of the BBB strongly indicates the presence of unique water dynamics essential for brain function. On the basis of the highly specific localization of AQP-4, namely, astrocyte end feet at the glia limitans externa and pericapillary Virchow–Robin space, we hypothesized that the AQP-4 system serves as an interstitial fluid circulator, moving interstitial fluid from the glia limitans externa to pericapillary Virchow–Robin space to ensure proper glymphatic flow draining into the cerebrospinal fluid. The hypothesis was tested directly using the AQP-4 facilitator TGN-073 developed in our laboratory, and [^{17}O]H_2O JJ vicinal coupling proton exchange MRI, a method capable of tracing water molecules delivered into the blood circulation. The results unambiguously showed that facilitation of AQP-4 by TGN-073 increased turnover of interstitial fluid through the system, resulting in a significant reduction in [^{17}O]H_2O contents of cortex with normal flux into the cerebrospinal fluid. The study further suggested that in addition to providing the necessary water for proper glymphatic flow, the AQP-4 system produces a water gradient within the interstitial space promoting circulation of interstitial fluid within the BBB. ***NeuroReport*** **29:697–703 Copyright © 2018 The Author(s). Published by Wolters Kluwer Health, Inc.**

NeuroReport 2018, **29**:697–703

Keywords: glia limitans externa, glymphatic flow, Virchow–Robin space, ***Xenopus laevis***

[a]Center for Integrated Human Brain Science, Brain Research Institute, University of Niigata, Niigata, Japan and [b]Department of Neurology, University of California, Davis, California, USA

Correspondence to Tsutomu Nakada, MD, PhD, FAAN, FANA, Center for Integrated Human Brain Science, Brain Research Institute, University of Niigata, 1 Asahimachi, Niigata 951-8585, Japan
Tel: + 81 252 270 677; fax: + 81 252 270 821; e-mail: tnakada@bri.niigata-u.ac.jp

*Vincent J. Huber and Hironaka Igarashi contributed equally to the writing of this article.

Received 7 December 2017 **accepted** 25 January 2018

Introduction

The presence of the blood–brain barrier (BBB) effectively isolates the brain from effects of the systemic environment. The main determinant of proper BBB functionality is the endothelium of brain capillaries [1,2], the unique structural properties of which restrict water access. In addition to lacking fenestrations, aquaporin-1 (AQP-1), a water channel abundantly expressed in endothelial cells of common capillaries, is actively suppressed in brain capillaries [3]. Claudin-2, a water channel expressed in the tight junctions of epithelium, is also not expressed in brain capillary endothelium tight junctions [4]. Brain capillary endothelium has been shown to have high electrical resistance, further confirming highly restricted water permeability [2,5].

The water channel subtype, aquaporin-4 (AQP-4), in contrast, is highly expressed in the brain, a discovery that has led to the erroneous interpretation that AQP-4 facilitates the flow of water into and out of the brain [6]. The presence of the BBB and the restriction of water movement preclude this possibility [2,7]. Indeed, in AQP-4 knockout animals, water entry into the BBB from the systemic circulation remains unchanged, although water entry into the cerebrospinal fluid (CSF) system is reduced [8,9]. It is now clearly understood that the functionality of AQP-4 is related to water dynamics within the BBB, independent from the systemic circulation [10].

Localization of AQP-4 in the brain is highly specific, existing virtually only on astrocyte end feet at the glia limitans externa (GLE) and pericapillary Virchow–Robin space (VRS) (Fig. 1) [8–10,14,15]. Interstitial fluid in VRS has its own circulation, referred to as 'interstitial flow', which plays a role similar to systemic lymphatics for the brain that lacks a conventional lymphatic system [16–19]. This latter system is now referred to as glymphatic flow (GF), denoting glial lymphatics, which drains into the CSF space [20–22]. The water dynamics within pericapillary VRS have been shown to be dependent on the functionality of AQP-4 [8–10].

AQP-4 on astrocyte end feet connects the intracellular space of astrocytes and extracellular (interstitial) space.

The study was in part presented at the Society of Neuroscience, 1-15 November 2017, Washington, DC, 745.01/C14.

Fig. 1

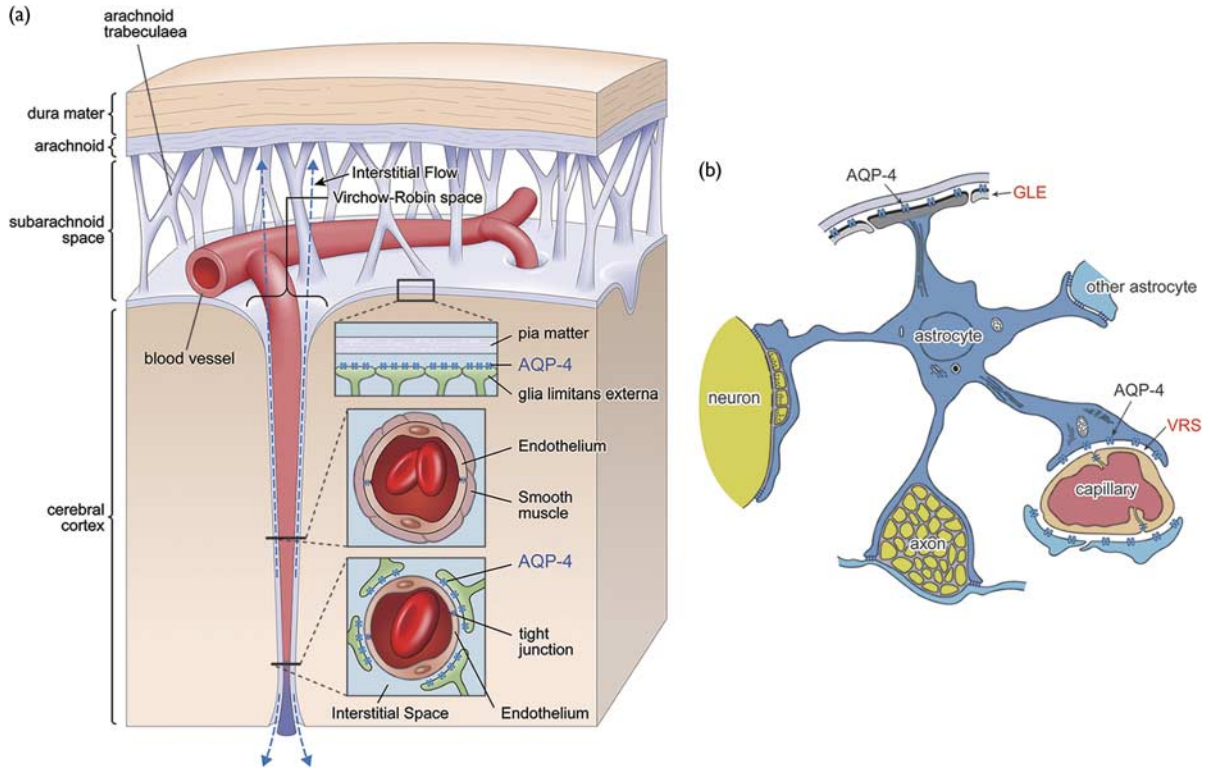

Schematic presentation of polarized localization of aquaporin-4 (AQP-4). (a) Relationship with Virchow–Robin space (VRS). Expression of AQP-4 in the brain is highly polarized to end feet of astrocytes at two specific locations: the glia limitans externa (GLE) at the cortical surface and pericapillary VRS. VRS constitutes fluid-filled canals surrounding perforating arteries and veins in the parenchyma of the brain. Although the pia mater ends near the brain surface, VRS continues into the brain parenchyma with a perforating artery. The arterial wall is surrounded by smooth muscle, which plays a main role in controlling capillary inner pressure (autoregulation), whereas the capillary is surrounded by interstitial fluid, the hydrodynamics of which are controlled by influx of water from intracellular fluid of astrocytes through AQP-4. (b) Astrocyte and end feet. Astrocyte end feet attach to many structures, but AQP-4 is found only at the GLE and the VRS. As AQP-4 at the capillary VRS is responsible for water efflux from astrocytes into VRS, it is highly plausible that AQP-4 at the GLE is responsible for water influx into the astrocyte from pericortical interstitial fluid space, thereby maintaining astrocyte intracellular water equilibrium. Diagram modified from Hirano [11] and Sasaki and Mannen [12], which show that a single astrocyte projects end feet both at the GLE and VRS [11,12]. Similar to the case of potassium siphoning, water homeostasis can be performed efficiently by a single astrocyte or may require a glia–cell syncytium [11,13].

As astrocyte intracellular fluid provides the water source for water influx into the interstitial space through AQP-4 at astrocyte end feet at VRS, to maintain intra-astrocyte water equilibrium, an equivalent amount of water has to enter the same astrocyte. The likely source is the only other AQP-4-rich site on astrocyte end feet at the GLE [10,23]. Similar to potassium siphoning and redistribution, water homeostasis can be sufficiently performed by a single astrocyte or, alternatively, may be dependent on a glia–cell syncytium [13,24]. In support of the former, it has indeed been shown that a single astrocyte directly connects the GLE and VRS [11,12].

Accordingly, we put forth the hypothesis that the AQP-4 system is an interstitial fluid circulator as described below. Using the AQP-4 facilitator TGN-073 developed in our laboratory, we directly tested the hypothesis in-vivo in mice by [^{17}O]H_2O JJ vicinal coupling proton exchange (JJVCPE) MRI, a method capable of tracing water molecules given into the blood circulation [9,25,26].

Materials and methods

Hypothesis

Interstitial fluid water of the GLE moves to pericapillary VRS through the intracellular fluid space of astrocytes, and, eventually drains into the CSF (Fig. 2) [10,23]. The hypothesis can be tested by quantitatively analyzing the effects of the AQP-4 facilitator TGN-073 on the water dynamics of the cortex, basal ganglia (BG), and CSF simultaneously by JJVCPE MRI following an injection of [^{17}O]H_2O into the systemic circulation.

Aquaporin-4 facilitator: TGN-073

Synthesis

The AQP-4 facilitator TGN-073, *N*-(3-benzyloxypyridin-2-yl)-benzene-sulfonamide (Fig. 3), was developed in our laboratory. TGN-073 was originally identified in our laboratory as a potential AQP-4 ligand on the basis of previously identified physicochemical properties conserved among other AQP-4 inhibitors [27].

Fig. 2

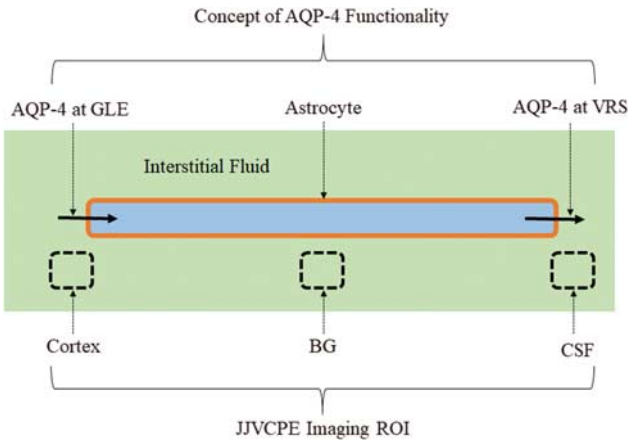

Schematic presentation of the aquaporin-4 (AQP-4) system. The AQP-4 system provides additional water flow into the pericapillary Virchow–Robin space (VRS). Necessary water enters astrocytes through AQP-4 at the glia limitans externa (GLE). This internal facilitator promotes appropriate interstitial fluid dynamics including flow through the VRS (interstitial flow), which constitutes glymphatic flow. This model is readily examined in-vivo by analyzing tracer dynamics injected into the systemic vein. Broken line squares indicate the components examined in the in-vivo dynamic studies using [^{17}O]H_2O JJ vicinal coupling proton exchange (JJVCPE) imaging and the AQP-4 facilitator, TGN-073 (Fig. 6).

Fig. 3

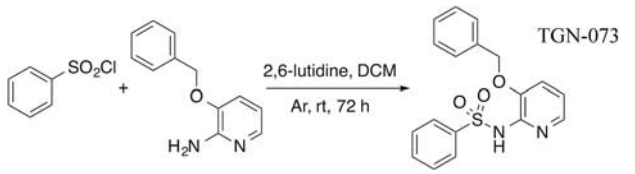

TGN-073 reaction schema.

In brief, reagents and solvents were sourced from Sigma-Aldrich (Tokyo, Japan), Wako Pure Chemical Industries (Osaka, Japan), TCI (Tokyo, Japan), or Nacalai Tesque Inc. (Kyoto, Japan) at the highest grade possible, and were used as received. Preparative flash chromatography was performed using a Wakogel 300 silica gel. ^{1}H nuclear magnetic resonance (^{1}H-NMR) spectra were recorded at 300 MHz on a Varian Mercury 300 spectrometer (Varian Inc., Palo Alto, California, USA) and are reported in parts per million downfield from an internal tetramethylsilane peak. Analytical ultraperformance liquid chromatography (UPLC) and high-resolution mass spectroscopy (HR-MS) were performed on a Waters Acquity UPLC (Milford, Massachusetts, USA) combined with a Waters LCT Premier XE mass detector. Additional UPLC analytical data were obtained using a Waters Acquity UPLC PDA detector. Analytical measurements were performed using an Acquity UPLC BEH C18 1.7 µm 2.1 × 50 mm column (waters) eluted with a 90–10% gradient of water/acetonitrile. Mass spectra were recorded in high-resolution mode.

Anhydrous dichloromethane (35 ml) was added to 2-amino-3-benzyloxypyridine (1.50 g, 7.5 mmol), followed by 2,6-lutidine (2.62 ml, 22.5 mmol). The resulting solution was blanketed with argon gas and stirred at room temperature for 5 min, following which, benzenesulfonyl chloride (1.05 ml, 8.25 mmol) was added, and the resulting solution was stirred for 72 h under argon gas (Fig. 3). Thereafter, the reaction mixture was washed with 10% aqueous citric acid (2 × 25 ml) and saturated with aqueous $NaHCO_3$ (2 × 25 ml); the organic solution was then dried over $MgSO_4$, filtered, and evaporated under reduced pressure to yield a dark brown solid (0.726 g). The crude solid was purified by flash chromatography (Wakogel 300, 1 : 2 ethyl acetate/hexane) to yield the desired product as a white solid. ^{1}H-NMR and UPLC-HR-MS were consistent with the assigned product, purity (UV) more than 95%. The material was used without further purification, 0.290 g (13%).

TGN-073 showed the following properties: ^{1}H-NMR (DMSO-D6): δ5.14 (s, ^{2}H), 6.90 (br-t, ^{1}H), 7.29–7.41 (m, ^{4}H), 7.47–7.64 (m, ^{6}H) 7.96 (br-d, $J = 6.6$ Hz, ^{2}H), 10.41 (br-s, ^{1}H). UPLC: rt = 1.72 min (DAD), and purity more than 95%. HR-MS: mass calculated for $C_{18}H_{17}N_2O_3S^+$ ($M + H^+$), 341.0955; found, 341.0932.

Xenopus laevis oocyte bioassay for confirming aquaporin-4 facilitation

The facilitation effect of TGN-073 on AQP-4 was confirmed using the bioassay described previously [28,29]. In brief, denuded stage V–VI oocytes were prepared from an adult, female *X. laevis*, and were allowed to equilibrate in modified Barth's medium (MBS) for ~12 h at 18°C before cRNA injection. AQP-4 cRNA solutions (0.1 µg/µl cRNA) for oocytye injection were prepared from an existing stock solution. An aliquot (30 nl) of either the cRNA solution or distilled water (sham) was injected into each oocyte using a Drummond oocyte injection system (Drummond Nanoject II; Drummond Scientific, Broomall, Pennsylvania, USA). Injected oocytes were then incubated for 48 h at 18°C in MBS. Medium was changed and nonviable oocytes were removed at 24 and 48 h after injection. Before the assay, 4–5 oocytes along with MBS (450 ml) were transferred to a single well of a 24 well-polystyrene plate (3526; Costar), to which an aliquot (50 µl) of TGN-073 stock solution (0.2 mM in 1% DMSO containing MBS) or a blank (1% DMSO in MBS) was added. Oocytes were incubated at 20°C for 30 min. Before imaging, the plate was transferred to an SZX16 zoom microscope (Olympus Corporation, Tokyo, Japan) fitted with a DP26 digital camera (Olympus Corporation) and a MATS-5555 temperature-controlled stage (Tokai Hit, Fujinomiya, Japan) set at 22°C. Hypotonic shock was initiated by introducing an equimolar TGN-073 solution or blank containing 0.1% DMSO, also maintained at 22°C. Single-well images were captured in

15-s intervals for 150 s following the addition of hypotonic medium. Images were transferred to a personal computer and the hypotonic response of 18–20 individual oocytes per test group was evaluated as described previously. Statistical significance was tested using a one-way analysis of variance with Fisher's least significant difference test. P values below 0.01 were considered significant.

JJVCPE imaging

The concept of the JJVCPE imaging method and its validation studies have been published previously [9,25]. The concept is schematically presented in Fig. 4.

Animal preparation

The study was approved by the Internal Review Board of University of Niigata and carried out in accordance with the Guidelines laid down by the NIH (USA) on the care and use of animals for experimental procedures. Five control and five study adult male mice, C57/BL6 (weight 23–28 g), were maintained under standard laboratory conditions under a 12/12 h light/dark cycle. Food and water were available *ad libitum*. Animals breathing spontaneously and anesthetized with an intraperitoneal administration of urethane (1.2 g/kg) were placed supine in a custom-designed Plexiglas stereotactic holder. The head was fixed in position by ear and tooth bars. Rectal temperature was maintained at 37 ± 0.5°C using a customized temperature control system. Oxygen saturation was monitored throughout the MR study using a pulse oxymeter Mouse Ox (Starr Life Sciences Co., Oakmont, Pennsylvania, USA), with probe placement on the left thigh. TGN-073 was administered intraperitoneally at a dose of 20 mg/kg (control dose) or 200 mg/kg (experimental dose) in 0.2 ml saline 30 min before the study. Normal saline of 0.2 ml was used for sham injection. For the dynamic imaging study, 0.2 ml normal saline containing 40% of $[^{17}O]H_2O$ (Isotec Inc., St Louis, Missouri, USA) was administered as an intravenous bolus injection at the 75th phase (10 min after the first scan) using an automatic injector at 0.04 ml/s through PE10 tubing inserted into the right femoral vein.

Data acquisition

MRI experiments were conducted on a 15-cm bore 7 T horizontal magnet (Magnex Scientific, Abingdon, UK) using a Varian Unity-INOVA-300 system (Varian Inc., Palo Alto, California, USA) equipped with an actively shielded gradient. A custom-made one turn surface coil, 20 mm outer diameter, was used for RF transmission. Adiabatic double-spin echo-prepared rapid acquisition with refocused echoes was utilized at the following parameter settings: single slice (2 mm thick), 128 × 128 matrix image of 20 × 20 mm, field of view every 8 s, TR 2000 ms, echo train 32, TE for the first echo 8.8 ms, echo spacing 5 ms, and effective TE 84.8 ms. Imaging slabs were set 6 mm caudal from the top of the cerebrum. A total of 525 phases (scan time 70 min) were obtained at 8 s intervals.

Fig. 4

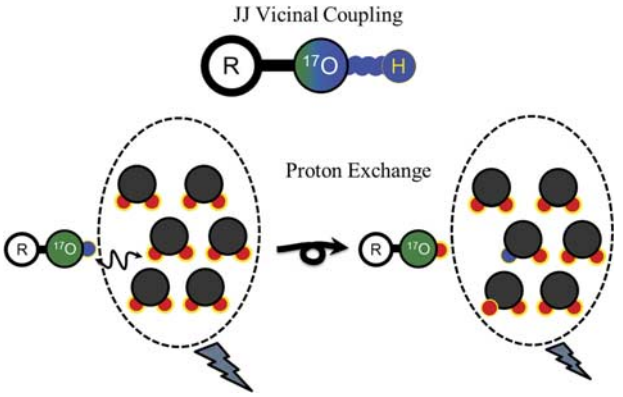

Schematic presentation of JJ vicinal coupling proton exchange (JJVCPE) imaging. The nuclear magnetic resonance (NMR)-sensitive, nonradioactive isotope of oxygen, oxygen-17 [^{17}O], and adjacent proton will show JJ vicinal coupling. In water, the protons of the water molecule and ionized proton of the dissolved molecule can exchange among each other. Accordingly, appropriately designed [^{17}O]-labeled molecules can alter the apparent T2 of water molecules under NMR experiments. Using T2-weighted imaging, this can be developed into noninvasive imaging, JJVCPE imaging that is capable of quantifying the contents of the target molecules, akin to radioactive tracer imaging such as PET [9,25].
Signal intensity change, δS, of the voxel with [^{17}O]-labeled substrate can be given by:

$$\delta S = S_0\left(1-\exp\left\{-\mathrm{TE}\left[\frac{1}{\mathrm{T2}}+\frac{35}{12}\rho\tau J^2\right]\right\}\right),$$

where S_0 is the original signal intensity, TE is the echo time, ρ is the relative concentration of the [^{17}O]-labeled substrate, and τ is the proton exchange rate. Although it is difficult to determine the absolute concentration of the [^{17}O]-labeled target molecule with this imaging method, it is still possible to obtain dynamic data for a target molecule in space and time, given the high spatial resolution inherent to MRI. In contrast to radiotracer methods, tracer ([^{17}O]-labeled target molecule) contents have an inversed correlation with signal intensities, namely, higher tracer contents yield lower signal intensities.

Data analysis

Images were analyzed using image processing software (MR vision; MR Vision Co., Winchester, Massachusetts, USA). Averaged percent intensities, which reflect the relative influx of $[^{17}O]H_2O$ in three areas, the cortex, the BG, and the third ventricle, were plotted against time. Intensities at the steady state of each area, expressed as percentage against the averaged intensity of identical pixel before administration of $[^{17}O]H_2O$, were determined by fitting their time course by the function (Fig. 5a):

$$I = I_0 + ae^{-bt}.$$

Representative in-vivo data from control mouse are shown in Fig. 5b.

Statistics

Numerical data were subjected to a Student t-test for the raw data using commercial statistical software (SPSS 24, Armonk, New York, New York, USA). The value of P

Fig. 5

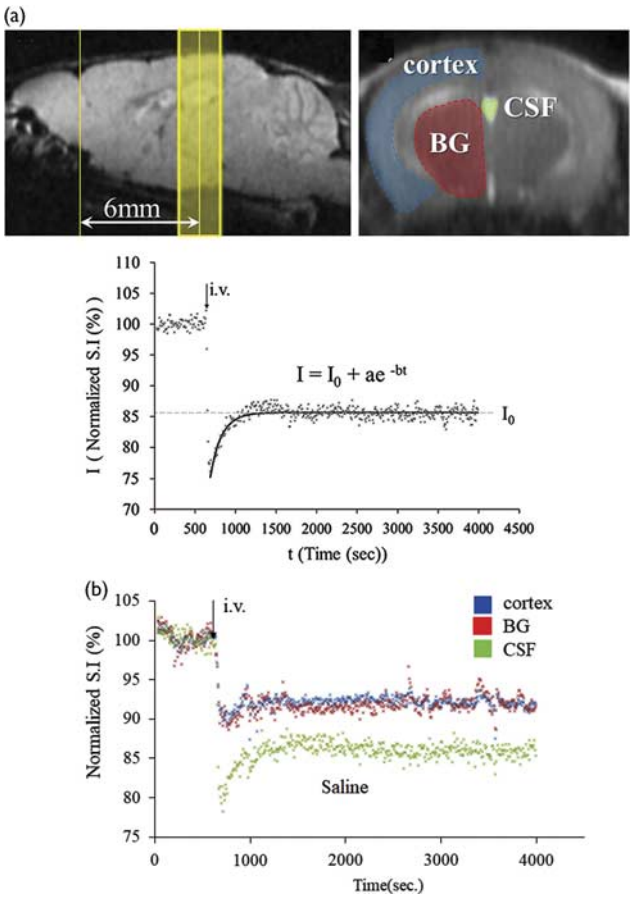

JJVCPE data. (a) ROI and decay curve fitting. Upper: scout film showing regions of interest (ROI). Imaging slab was set to 6 mm caudal from the top of the cerebrum (left) and ROI was selected semiautomatically using image processing software. Lower: Decay curve fitting. I_0 shows the normalized signal intensity at infinite time ($t = \infty$) calculated from the fitted curve. As described, higher tracer contents will yield lower I_0. (b) Representative time course. Representative time curve of signal intensities within pixels of each ROI shown in (a) following intravenous (i.v.) [^{17}O]H_2O administration in control mouse. Blue: cortex, red: basal ganglia (BG), green: cerebrospinal fluid (CSF) within the third ventricle. Each dot represents the intensity of each pixel within the ROI.

less than 0.05 was considered statistically significant. All data were shown as mean ± SD ($n = 5$).

Results

TGN-073

AQP-4 expressing oocytes treated with 10 μM TGN-073 were observed to have a greater AQP-4-mediated increase in volume following hypotonic shock compared with identically prepared oocytes treated with a blank (Fig. 6a). On the basis of the volumetric changes between 0 and 150 s, the mean fluxes (P_f) of 12 ± 0.5, 80 ± 3, and 96 ± 3 × 10^{-4} cm/s were determined for the sham, blank, and TGN-073 groups, respectively (Fig. 6b). Incubation with TGN-073 led to a significant increase in AQP4-mediated water flux ($P < 0.005$, one-way analysis of variance with Fisher's least significant difference test), confirming that TGN-073 is indeed an AQP-4 facilitator.

Fig. 6

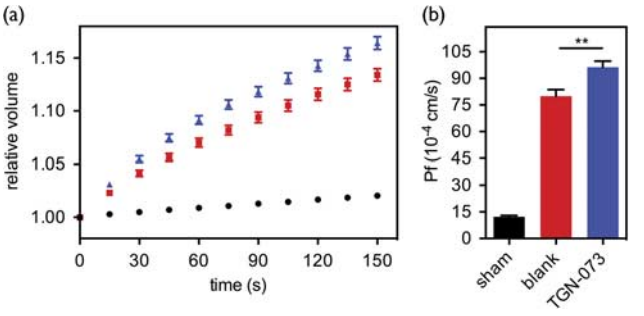

Xenopus laevis oocyte bioassay. (a) Time-dependent volume change plots are shown for water-injected oocytes incubated for 30 min before initiation of hypotonic shock with a blank (black circle), and AQP-4 cRNA-injected oocytes incubated with a blank (red square) or TGN-073 (blue triangle). (b) Hypotonic flux (P_f) of the sham, blank, and TGN-073 groups is shown as black bars plus SEM. Statistical significance between the blank and TGN-073 groups is indicated by $^{**}P = 0.0025$ (one-way analysis of variance with Fisher's least significant difference test).

JJ vicinal coupling proton exchange imaging

Results showing the effects of TGN-073 are summarized in Fig. 7. A significant reduction in the tracer ([^{17}O]H_2O) content ($P < 0.005$, Student-t, $n = 5$) was found in the cortex, indicating higher turnover of interstitial fluid of the cortex associated with AQP-4 facilitation. As expected, the tracer content was not affected significantly in the BG because of the lack of AQP-4. Tracer content is inherently much higher in the CSF and the relatively minor facilitation in AQP-4 as shown in Fig. 6 cannot be expected to alter MRI signals significantly. The result validated the presented hypothesis of interstitial fluid circulation (Fig. 2).

Discussion

The current study represents the first report of a pharmacological agent capable of increasing water flux through AQP-4 (AQP-4 facilitator), that is, TGN-073. AQP-4 is a bidirectional water channel. It is believed to be regulated by proton density (pH) [30]. Nevertheless, in contrast to the case of inhibitors, the mechanisms of which could be defined rather simply as channel blockade, the mechanism of TGN-073-mediated AQP-4 facilitation is not intuitive. It can, however, logically be speculated that ligand interaction with AQP-4 leads to a conformational shift, especially in the protein loop spanning the H2 and HB helices, which results in facilitation of water flux [30].

On the basis of AQP-4 structural analysis for its regulatory process by protons, restriction in the motion of that loop following the protonation of H95 has been suggested to be the reason for increased AQP-4 flux at low pH [25].

Fig. 7

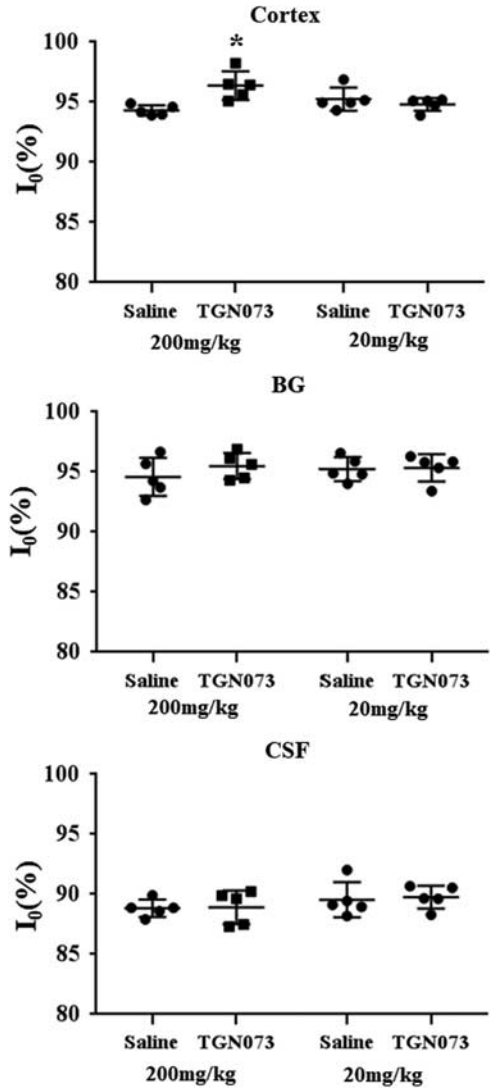

Group analysis of TGN-073 effect. Group treated with an experimental dose of TGN-073 (200 mg/kg) showed significantly higher I_0 in the cortex compared with the saline-treated group, indicating higher turnover of $[^{17}O]H_2O$ in the cortex. The group treated with a control dose of TGN-073 (20 mg/kg) did not show any significant effects, excluding potential nonspecific effects of TGN-073.*$P = 0.0066$ (*t*-test). BG, basal ganglia; CSF, cerebrospinal fluid.

Although the events giving rise to these conformational restrictions, that is, pH changes and ligand binding, are different, it is plausible to consider that the relative increases in AQP-4 flux reported in the present study are based on similar changes in the H2-HB spanning loop. In any event, the bioassay reported in this study unambiguously showed that TGN-073 can facilitate AQP-4 water flux *in vivo*.

Studies to date have not identified any specific passage for water into the BBB. Water entry into the BBB is therefore a nonspecific, presumably slow movement through the lipid membrane as it had been believed before the discovery of water-specific channels [31]. Indeed, $[^{17}O]H_2O$ JJVCPE MRI studies of normal and AQP-4 knockout mice have consistently shown that ~20 min are necessary to reach the steady state of the $[^{17}O]H_2O$ concentration for structures inside the BBB following an intravenous bolus injection of $[^{17}O]H_2O$ irrespective of the presence or absence of AQP-1 or AQP-4 [9,26]. The current study unambiguously confirmed the notion by showing that facilitation of AQP-4 does not alter gross transport of $[^{17}O]H_2O$ from the blood stream to CSF. However, facilitation of AQP-4 significantly increases the turnover of water from cortical areas into pericapillary VRS (Fig. 2).

It has long been recognized that interstitial fluid within VRS has its own circulation, transferring the fluid from the pericapillary space into the CSF system through the VRS system surrounding perforating arteries and veins in the parenchyma of the brain [19,32,33]. The importance of this 'third circulation' in the brain, which is now referred to as GF, is believed to be the equivalent of systemic lymphatics and responsible for β-amyloid clearance [19–22,33,34]. Pericapillary water dynamics and, hence, GF functionality are dependent on the AQP-4 system. Therefore, disturbance of AQP-4 function and the resultant GF dysfunction are now believed to play a significant, if not sole, role in the pathogenesis of Alzheimer's disease (AD). Indeed, patients with AD are shown to have impaired GF [35].

The current study unambiguously showed that the AQP-4 system indeed works as an interstitial circulator (Fig. 2), and facilitation of AQP-4 by TGN-073 increased turnover of interstitial fluid from the cortical area. Should aging-oriented AQP-4 dysfunction be the main pathogenesis of AD, it would translate into the notion that AD is not simply a 'β-amyloid accumulation' disease. Disruption in interstitial circulation because of AQP-4 functionality dysfunction would adversely impact nutrient delivery, neural excitability, and even regional perfusion. The implications of these processes on the pathologic cascade add to the complexity of the pathogenesis of AD. Therefore, facilitation of AQP-4 functionality is a promising pharmacologic target in the prevention and treatment of AD.

Acknowledgements

The work was supported by grants from the Ministry of Education, Culture, Sports, Science, and Technology (Japan).

Conflicts of interest

There are no conflicts of interest.

References

1 Reese TS, Karnovsky MJ. Fine structural localization of a blood–brain barrier to exogenous peroxidase. *J Cell Biol* 1967; **34**:207–217.

2 Weiss N, Miller F, Cazaubon S, Couraud PO. The blood–brain barrier in brain homeostasis and neurological diseases. *Biochim Biophys Acta* 2009; **1788**:842–857.
3 Dolman D, Drndarski S, Abbott NJ, Rattray M. Induction of aquaporin 1 but not aquaporin 4 messenger RNA inrat primary brain microvessel endothelial cells in culture. *J Neurochem* 2005; **93**:825–833.
4 Rosenthal R, Milatz S, Krug SM, Oelrich B, Schulzke JD, Amasheh S, *et al.* Claudin-2, a component of the tight junction, forms a paracellular water channel. *J Cell Sci* 2010; **123**:1913–1921.
5 Günzel D, Yu ASL. Claudins and the modulation of tight junction permeability. *Physiol Rev* 2013; **93**:525–569.
6 Papadopoulos MC, Verkman AS. Aquaporin water channels in the nervous system. *Nat Rev Neurosci* 2013; **14**:265–277.
7 Abbott NJ, Ronnback L, Hansson E. Astrocyte–endothelial interactions at the blood–brain barrier. *Nat Rev Neurosci* 2006; **7**:41–53.
8 Haj-Yasein NN, Jensen V, Østby I, Omholt SW, Voipio J, Kaila K, *et al.* Aquaporin-4 regulates extracellular space volume dynamics during high-frequency synaptic stimulation: a gene deletion study in mouse hippocampus. *Glia* 2012; **60**:867–874.
9 Igarashi H, Tsujita M, Kwee IL, Nakada T. Water influx into cerebrospinal fluid (CSF) is primarily controlled by aquaporin-4, not by aquaporin-1: O-17 JJVCPE MRI study in knockout mice. *Neuroreport* 2014; **25**:39–43.
10 Nakada T, Kwee IL, Igarashi H, Suzuki Y. Aquaporin-4 functionality and Virchow–Robin space water dynamics: physiological model for neurovascular coupling and glymphatic flow. *Int J Mol Sci* 2017; **18**:1798.
11 Hirano A. Astrocyte: neuropathological viewpoint. In: Ikuta F, editor. *Glial cells*. Tokyo: KubaPro; 1999. pp. 111–131.
12 Sasaki H, Mannen H. Morphological analysis of astrocytes in the bull frog (*Rana catesbeiana*) spinal cord with special reference to the site of attachment of their processes. *J Comp Neurol* 1981; **198**:13–35.
13 Newman EA. Regulation of extracellular K^+ and pH by polarized ion fluxes in glial cells: the retinal Muller cell. *Neuroscience* 1996; **2**:109–117.
14 Rash JE, Yasumura T, Hudson CS, Agre P, Nielsen S. Direct immunogold labeling of aquaporin-4 in square arrays of astrocyte and ependymocyte plasma membranes in rat brain and spinal cord. *Proc Natl Acad Sci USA* 1998; **95**:11981–11986.
15 Neely JD, Christensen BM, Nielsen S, Agre P. Heterotetrameric composition of aquaporin-4 water channels. *Biochemistry* 1999; **38**:11156–11163.
16 Esiri MM, Gay D. Immunological and neuropathological significance of the Virchow–Robin space. *J Neurol Sci* 1990; **100**:3–8.
17 Weller RO. Pathology of cerebrospinal fluid and interstitial fluid of the CNS: significance for Alzheimer's disease, prion disorders and multiple sclerosis. *J Neuropathol Exp Neurol* 1998; **57**:885–894.
18 Johnston M, Papaiconomou C. Cerebrospinal fluid transport: a lymphatic perspective. *News Physiol Sci* 2002; **17**:227–230.
19 Abbott NJ. Evidence for bulk flow of brain interstitial fluid: significance for physiology and pathology. *Neurochem Int* 2004; **45**:545–552.
20 Xie L, Kang H, Xu Q, Chen MJ, Liao Y, Thiyagarajan M, *et al.* Sleep drives metabolite clearancefromthe adult brain. *Science* 2013; **342**:373–377.
21 Iliff JJ, Wang M, Liao Y, Plogg BA, Peng W, Gundersen GA, *et al.* A paravascular pathwayfacilitatesCSF flow throughthe brain parenchymaandthe clearanceof interstitial solutes, including amyloidβ. *Sci Transl Med* 2012; **4**:147ra111.
22 Nakada T. Virchow–Robin space and aquaporin-4: new insights on an old friend. *Croat Med J* 2014; **55**:328–336.
23 Suzuki K, Yamada K, Nakada K, Suzuki Y, Watanabe M, Kwee IL, Nakada T. MRI characteristics of the glia limitans externa: a 7T study. *Magn Reson Imaging* 2017; **44**:140–145.
24 Kofuji P, Newman EA. Potassium buffering in the central nervous system. *Neurosci* 2004; **129**:1045–1056.
25 Suzuki K, Igarashi H, Huber VJ, Kitaura H, Kwee IL, Nakada T. Ligand based molecular MRI: O-17 JJVCPE amyloid imaging in transgenic mice. *J Neuroimg* 2014; **24**:595–598.
26 Igarashi H, Suzuki Y, Kwee IL, Nakada T. Water influx into cerebrospinal fluid is significantly reduced in senile plaque bearing transgenic mice, supporting ß-amyloid clearance hypothesis of Alzheimer disease. *Neurological Res* 2014; **36**:1094–1098.
27 Suzuki Y, Nakamura Y, Yamada K, Huber VJ, Tsujita M, Nakada T. Aquaporin-4 positron emission tomography imaging of the human brain: first report. *J Neuroimaging* 2013; **23**:219–223.
28 Huber VJ, Tsujita M, Kwee IL, Nakada T. Inhibition of aquaporin 4 by antiepileptic drugs. *Bioorg Med Chem* 2009; **17**:418–424.
29 Huber VJ, Tsujita M, Nakada T. Identification of aquaporin 4 inhibitors using in vitro and in silico methods. *Bioorg Med Chem* 2009; **17**:411–417.
30 Kaptan S, Assentoft M, Schneider HP, Fenton RA, Deitmer JW, MacAulay N, de Groot BL. H95 is a pH-dependent gate in aquaporin 4. *Structure* 2015; **23**:2309–2318.
31 Mathai JC, Tristram-Nagle S, Nagle JF, Zeidel ML. Structural determinants of water permeability through the lipid membrane. *J Gen Physiol* 2008; **131**:69–76.
32 Virchow R. Ueber die Erweiterung kleinerer Gefaesse. *Arch Pathol Anat Physiol Klin Med* 1851; **3**:427–462.
33 Robin C. Recherches sur quelques particularites de la structure des capillaires de l'encephale. *J Physiol Homme Animaux* 1859; **2**:537–548.
34 Tarasoff-Conway JM, Carare RO, Osorio RS, Glodzik L, Butler T, Fieremans E, *et al.* Clearance systems in the brain-implications for Alzheimer disease. *Nat Rev Neurol* 2015; **11**:457–470.
35 Suzuki Y, Nakamura Y, Yamada K, Igarashi H, Kasuga K, Yokoyama Y, *et al.* Reduced CSF water influx n Alzheimer's disease supporting the ß-amyloid clearance hypothesis. *PLoS One* 2015; **10**:e0123708.